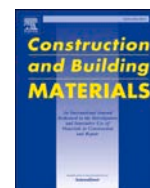




Contents lists available at ScienceDirect

## Construction and Building Materials

journal homepage: [www.elsevier.com/locate/conbuildmat](http://www.elsevier.com/locate/conbuildmat)

## The key to ancient Roman mortars hydraulicity: ceramic fragments or volcanic materials? A lesson from the Phlegraean archaeological area (southern Italy)

Concetta Rispoli<sup>a,b,\*</sup>, Giovanna Montesano<sup>a</sup>, Maria Verde<sup>c</sup>, Giuseppina Balassone<sup>a,b</sup>, Stefano Columbu<sup>d</sup>, Alberto De Bonis<sup>a,b</sup>, Claudia Di Benedetto<sup>a</sup>, Francesco D'Uva<sup>a</sup>, Renata Esposito<sup>e</sup>, Sossio Fabio Graziano<sup>b,f</sup>, Mariano Mercurio<sup>b,g</sup>, Vincenzo Morra<sup>a,b</sup>, Piergiulio Cappelletti<sup>a,b,h</sup>

<sup>a</sup> Dipartimento di Scienze della Terra, dell'Ambiente e delle Risorse (DiSTAR), Università degli Studi di Napoli Federico II, Via Cupa Nuova Cintia 21, 80126 Napoli, Italy

<sup>b</sup> Center for Research on Archaeometry and Conservation Science - CRACS, Complesso Universitario di Monte Sant'Angelo, Via Cupa Nuova Cintia, 21, 80126 Napoli, Italy

<sup>c</sup> Dipartimento di Architettura, Università degli Studi di Napoli Federico II, Via Forno Vecchio, 36, 80134 Napoli, Italy

<sup>d</sup> Dipartimento di Scienze Chimiche e Geologiche, Università degli Studi di Cagliari, Blocco A, Cittadella universitaria, 09042 Monserrato, Italy

<sup>e</sup> Dipartimento di Studi Umanistici, Università degli Studi di Napoli Federico II, Via Porta di Massa 1, 80133 Naples, Italy

<sup>f</sup> Dipartimento di Farmacia, Università degli Studi di Napoli Federico II, via D. Montesano 49, 80131 Napoli, Italy

<sup>g</sup> Dipartimento di Scienze e Tecnologie, Università degli Studi del Sannio, Via De Sanctis, Benevento 82100, Italy

<sup>h</sup> Centro Musei delle Scienze Naturali e Fisiche, Università degli Studi di Napoli Federico II, Napoli, Italy

## ARTICLE INFO

## Keywords:

Roman mortars  
Phlegraean Fields  
Hydraulic mortars  
Ceramic  
cocciopesto  
Aggregate  
Reactivity

## ABSTRACT

This research deals with mineralogical, petrographic, chemical, and microstructural characterization of raw materials from the Roman *Dragonara* cave (Phlegraean Fields, Campania region, Italy) through Polarized Light Microscopy (PLM), X-ray Powder Diffraction (XRPD), Field Emission Scanning Electron Microscopy coupled with an Energy Dispersive Spectrometer (FESEM/EDS), Simultaneous Thermal Analysis (STA) and Mercury Intrusion Porosimetry (MIP). The aim of this study was to assess mortars hydraulic properties along with provenance of raw materials and mortars recipe. A focus on the reactions between the surface of the ceramic aggregates and volcanic materials with binding matrix proved to be crucial to define their role in the mix design of mortars. Representative results showed that hydraulicity of the analyzed mortars is mainly due to volcanic materials rather than ceramic fragments. In fact, reaction active elements such as Reaction Rims (RR), Interfacial Transition Zones (ITZ) and particularly Ca-rich rims were usually found at the matrix-volcanic fragments interface. Moreover, porosity tests evidence that bedding mortars, which contain mainly volcanic material and only sporadically ceramic fragments have a higher closed porosity of binder matrix due to the good pozzolanic reactivity.

## 1. Introduction

The manufacturing of mortars can be considered such an art that began in historical times. Ancient authors, such as Pliny the Elder, described practical instructions to produce and mix ingredients such as lime, known since Egyptians. However, a wide diffusion of these geo-materials, and especially the innovations in the production technologies, notably occurred in the Roman Empire. Mortars are composite

geological-based materials of high complexity due to their variable composition which is strictly connected to local techniques and traditions, as well as changes over time by interaction with the environment. They may play several roles in the masonry such as bedding mortars, plasters, bonding of ceramic tiles or pavements.

The ancient Romans initially used mainly aerial lime as a binder. The hardening of mortars occurred very slowly (today we would say “slow setting”) as regards aerial lime binder, because the lime consolidation is

\* Corresponding author at: Dipartimento di Scienze della Terra, dell'Ambiente e delle Risorse (DiSTAR), Università degli Studi di Napoli Federico II, Via Cupa Nuova Cintia 21, 80126 Napoli, Italy.

E-mail address: [concetta.rispoli@unina.it](mailto:concetta.rispoli@unina.it) (C. Rispoli).

<https://doi.org/10.1016/j.conbuildmat.2023.134408>

Received 21 June 2023; Received in revised form 14 November 2023; Accepted 30 November 2023

0950-0618/© 2023 The Author(s). Published by Elsevier Ltd. This is an open access article under the CC BY license (<http://creativecommons.org/licenses/by/4.0/>).

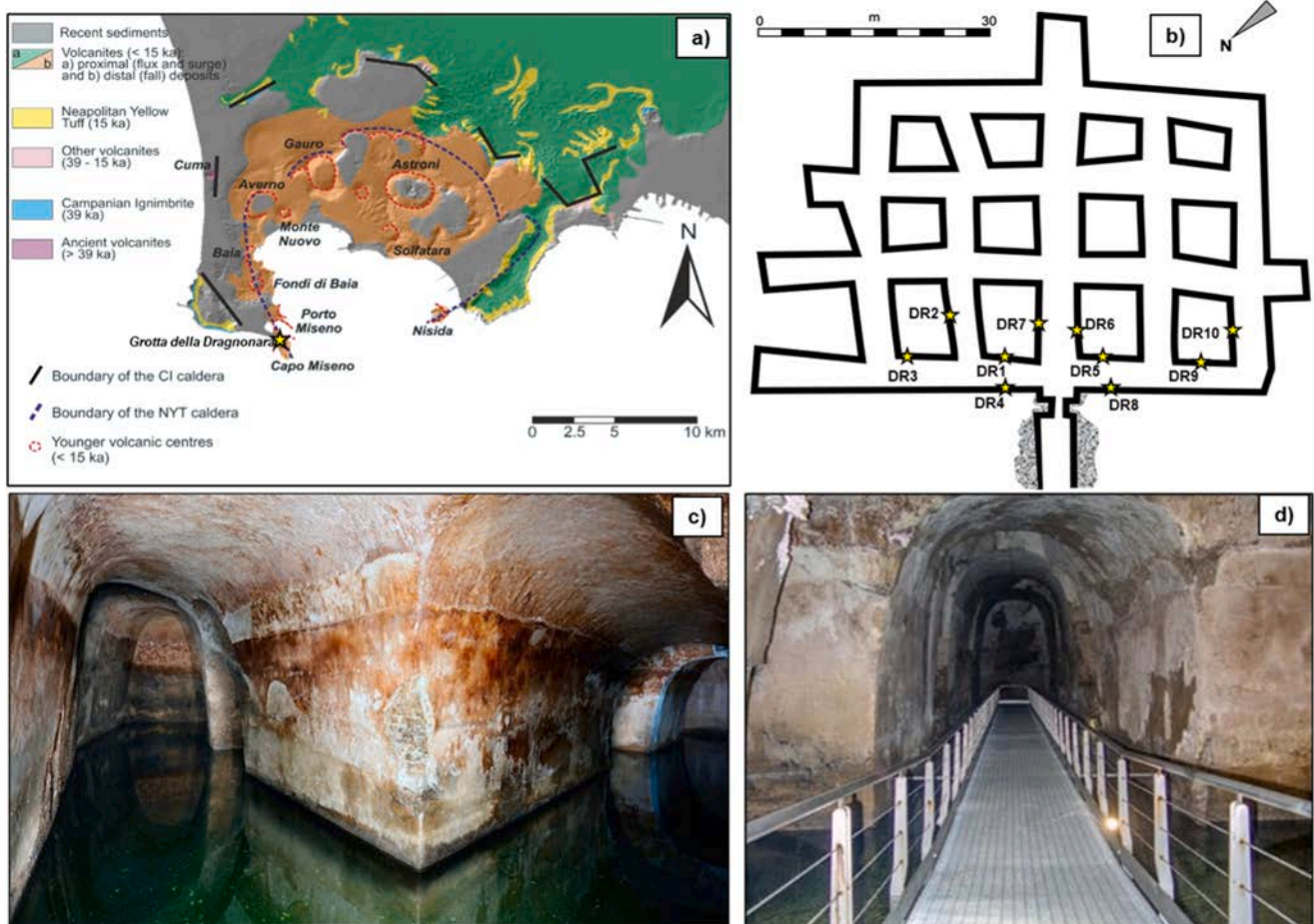


Fig. 1. A) Geological sketch map of Phlegraean Fields (modified after [31]). B) Sketch map of the *Dragonara* cave with sampling points (modified after Amalfitano et al., 1990). C-d) Interior of *Dragonara* cave.

due to the reaction of  $\text{Ca}(\text{OH})_2$  with  $\text{CO}_2$  in the air, producing  $\text{CaCO}_3$  [1].

From the 1st century BCE, Roman craftsmen guessed that the combination of lime with a specific volcanic sandy material, called *pozzolana* (in latin *Pulvis Puteolana*, literally powder from *Pozzuoli*, a typical deposit related to Neapolitan Yellow Tuff eruption of 15.000 years ago [2]) led mortars and concretes to become hydraulic, allowing underwater hardening and increasing their mechanical strength [3–5]. Thanks to the recombination of aluminosilicate provided by *pozzolana* and  $\text{Ca}(\text{OH})_2$  in aqueous solution, hydration reaction produces calcium silicate and calcium aluminate hydrates, the so-called C-A-S-H gel [6].

Whether volcanic material was not available, fragments of artificial materials (e.g., ceramic fragments), having similar hydraulic properties as *pozzolana*, were used. The mortars made with ceramic fragments are called *cocciopesto* and these were preferred in water-bearing structures and to protect the walls from moisture, typically in baths, canals, and aqueducts [7–12].

This innovation in the mortars production technology can be linked to the most current research themes such as sustainability and recycling. Previous studies [13,14] highlighted that ceramic fragment used within the *cocciopesto* are different in terms of optical activity (birefringence), petrographic characteristics, and texture. This led to hypothesize that they derive from recycled material from different ceramic productions and allegedly represents the first example of reuse and recycling in history [13,14].

Several studies [15–19] were carried out on Roman mortars and ceramic artifacts, whereas less attention has been focused on the ceramic

fragments used in hydraulic mortars.

The *Dragonara* cave is a Roman cistern located in the Phlegraean Fields Archaeological Park. Thanks to its geographical position, the *Dragonara* cave offers the most suitable conditions to carry out a study about the manufacturing of Roman mortars due to its proximity to the ancient *pozzolana* quarries. In addition to the *pozzolana* used for the mortars, ceramic fragments were also discovered as a construction material of the cistern. Therefore, the aim of this work is to characterize for the first time the Roman mortars from this important archaeological site in order to: 1) define provenance of raw materials and recipe and 2) assess hydraulic properties with a specific focus on the reactions between the surface of the ceramic aggregates and volcanic materials with binding matrix.









## 2. Geological and archaeological background

The *Dragonara* cave is located in the Phlegraean Fields Area (CFA) (Fig. 1a), an area of the volcanic district in the western part of the city of Naples, also including *Ischia* and *Procida* islands. Its volcanic history is characterized by several eruptions from mainly monogenetic volcanic edifices that emplaced pyroclastic deposits and sporadic lava flows [20, 21].

Phlegraean Fields volcanism starts in the Upper Pleistocene, dating back to 80 ka deposits exposed at *Monte di Procida* and *Procida* Island, *San Severino*, *Punta Marmolite*, at the eastern border of *Piano di Quarto*, *Camaldoli*, in the urban area of Naples, *San Martino Hill* [22] *Castel*



**Table 1**

List and brief macroscopic description of the examined mortar according to UNI EN 11305 [34] and UNI EN 12407 [35].

Sample	Typology	Binder colour	Aggregate size	Cohesion	Petrographic lithotype
DR1	Coating mortar	Beige	Up to 1 cm	+++	
DR2	Coating mortar	light beige	Up to 1.5 cm	+++	
DR3	Coating mortar	whitish	Up to 1 cm	+++	
DR4	Coating mortar	beige	Up to 1 cm	++	
DR5	Coating mortar	light beige	Up to 1.5 cm	+++	
DR6	Coating mortar	beige	Up to 1 cm	++	
DR7	Bedding mortar	light brown	Up to 0.5 cm	++	
DR8	Bedding mortar	light brown	Up to 0.5 cm	++	

*(continued on next page)*

Table 1 (continued)

Sample	Typology	Binder colour	Aggregate size	Cohesion	Petrographic lithotype
DR9	Coating mortar	whitish	Up to 1 cm	++	
DR10	Coating mortar	light beige	Up to 1 cm	+++	

-1 cm

Cohesion: + + +, high; + +, medium; (i.e., the cohesion has been evaluated to the touch, depending on the crumbling of the material).

dell'Ovo and Capodimonte, whereas the southern sector of Phlegraean Fields is today submerged in the Pozzuoli Gulf.

The two high-magnitude eruptions of Phlegraean Fields represented by the Campanian Ignimbrite (CI, ~ 39.8 ka [23] and the Neapolitan Yellow Tuff (NYT, 15.4 ka) [2,24]. CI event is the most powerful eruption of Phlegraean Fields, which emplaced a widespread pyroclastic fall and flow sequence and caused a large caldera collapse encompassing Phlegraean Fields and Naples [25]. Post caldera volcanism, developed with tuff and scoriae cones along the caldera border (i.e., *Trentaremi* tuff ring, *Torregaveta* vent, *Monte di Procida*, *Solchiaro* tuff ring and *Procida* island; [26] and references therein), occurs before the NYT (Neapolitan Yellow Tuff) eruption. NYT eruption emplaced a large volume of pyroclastic deposits both lithified (due to zeolitization processes and representing the NYT s.s.) and massive (called "pozzolana"; [27]).

After some inactivity periods, other explosive eruptions both at the caldera borders (i.e., *Soccavo*, *Pianura*, *Agnano*, *Porto Miseno*, *Bacoli*, *Baia* and *Fondi di Baia*; [28] and in the central area of the caldera, as well as *Capo Miseno* and *Nisida*, took place.

Located at the eastern end of the beach of *Capo Miseno*, the *Dragonara* cave (from the latin "tracon" which means "rocky"; Fig. 1b) is a large Roman cistern dug into the tuffaceous promontory [29]. The cistern is about 60 m length, 50 m wide and 3.5–7 m high and has a quadrangular plan divided into five naves by four rows of pillars carved out in the tuff, covered by the "opus reticulatum" and by hydraulic "cocciopesto" [30] (Fig. 1b, c and d). The cistern was accessible originally only from the above through openings in the barrel vault (supplied with stairs) and used to the water introduction and maintenance. Nowadays the cistern is partly submerged because of the bradyseism, therefore a suspension bridge allows people to get inside.

### 3. Materials and methods

Ten mortar samples, consisting of eight coating mortars and two bedding mortars (Table 1 and Fig. 1b), were collected according to recommendation of the Archaeological Park of Phlegraean Fields and in collaboration with archaeologists. The sampling strategy was performed after an accurate on-site survey to define the most representative samples in terms of archaeological and architectural significance. For safety reasons it was possible to sample only one sector of the structure.

Experimental investigations were performed at the DiSTAR (*Dipartimento di Scienze della Terra, dell'Ambiente e delle Risorse, Università Federico II di Napoli*) and DST (*Dipartimento di Scienze e Tecnologie, Università del Sannio*).

Petrographic analysis was carried out on thin sections via PLM with a Leica Laborlux 12 pol microscope. To evaluate mineralogical composition of binder, aggregate, ceramic fragment and neo-formed phases, a mechanical separation was carried out according to the UNI-EN 11305

recommendation.

Qualitative mineralogical composition of samples was obtained by XRPD using a Panalytical X'Pert Pro diffractometer equipped with a RTMS X'Celerator detector (Cu-K $\alpha$  radiation, 40 kV, 40 mA, 2 $\theta$  range from 4° to 70° using a step interval of 0.017° 2 $\theta$ , with a step counting time of 120 s). The Panalytical Highscore Plus 3.0c software and PDF-2/ICSD databases were used to identify mineral phases.

Microstructural and chemical analyses of the investigated geomaterials, aimed to determine major elements chemical composition of binder and the lime lumps and to study ceramic fragments present as aggregates, were carried out by FESEM-EDS; Zeiss Merlin VP Compact and JEOL JSM-5310 coupled with Oxford Instruments Microanalysis Unit equipped with an INCA X-act solid state detector; (Carl-Zeiss-Strasse, Oberkochen, Germany and Jeol Ltd., Tokyo, Japan, respectively).

Data sets were obtained using an INCA X-max processor (Oberkochen, Germany) (15-kV primary beam voltage, 50–100 A filament current, from 30,000 to 200,000  $\times$  magnification, 20 mm working distance, and 50 s real-time counting) by means of INCA Energy software 5.05 (XPP array and pulse pile-up corrections). Optimization of signals was carried out using cobalt (FWHM peak height of the strobed zero = 60–65 eV) as a reference. Smithsonian Institute and MAC (Micro-Analysis Consultants Ltd., Saint Ives, UK) standard materials used for calibration and accuracies about EDS chemical analyses are reported in literature [14].

Furthermore, FESEM-EDS analyses were performed on areas with homogeneous appearance and with spots of 10  $\mu$ m for measuring hydraulicity index (HI) of binder and lime lumps. According to [32], the semiquantitative measure of HI accounts for the (SiO<sub>2</sub> + Al<sub>2</sub>O<sub>3</sub> + Fe<sub>2</sub>O<sub>3</sub>)/(CaO + MgO) ratio.

To determine the total (binder plus aggregates) hydraulicity index of these materials, thermal analyses (Thermogravimetric Analysis-TGA/Differential Scanning Calorimetry-DSC) were carried out. A Netzsch STA 449 F3 Jupiter thermal analyser coupled with a Netzsch Proteus 6.1.0, and Opus 7.0 software was used. Samples were placed in alumina crucibles and weight loss was monitored through a heating cycle from 40° to 1000°C with a temperature gradient of 10 °C/minute in an air-purged, silicon carbide furnace. This process reveals thermal transformations, such as dehydration, dihydroxylation, oxidation, and decomposition, thus providing quantitative information on binder compounds.

Connected porosity and pore size distribution were investigated by means of Mercury Intrusion Posimetry (MIP) on three representative sample fragments (DR1, DR7 and DR9) one for each petrographic group (PG) selected based on availability and macro-microscopic features. The specimens, with bulky volumes less than 5 cm<sup>3</sup>, were carefully broken off to avoid any changes in the natural distribution of the porous space



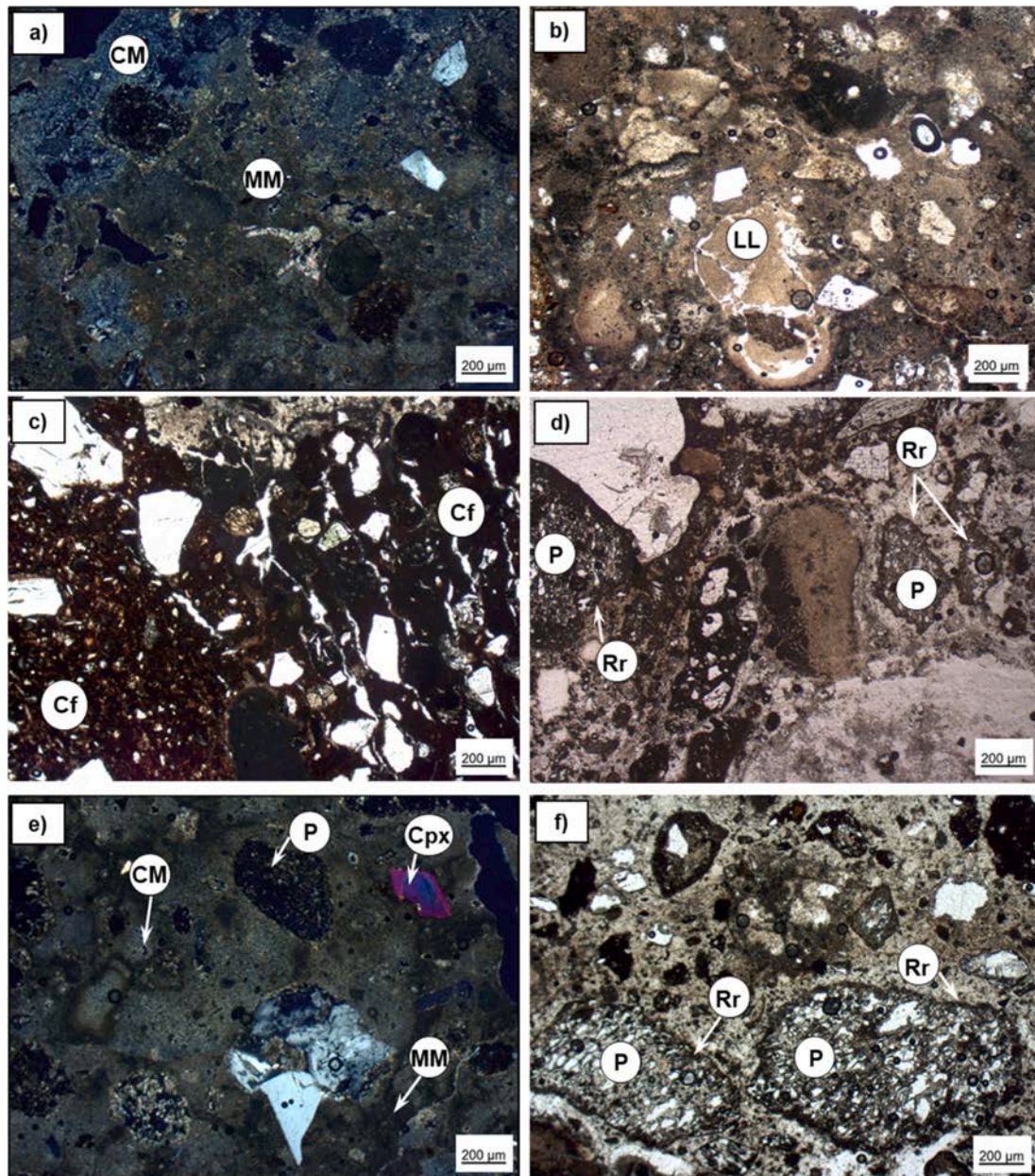


Fig. 2. Microphotographs of mortar components (in CPL: cross polarized light; PPL: plane polarized light). a) cryptocrystalline (CM) to micritic (MM) textured binder of the coating mortar (CPL); b) lime lump (LL), (PPL); c) ceramic fragments (Cf), (CPL); d) pumice (P) with reaction rims (Rr), (PPL); e) the micritic (MM) to cryptocrystalline (CM) matrix of bedding mortar, with a pumice (P) and a clinopyroxene (cpx) fragment (CPL); f) pumice (P) with reaction rims (Rr), (PPL).

and then dried for 24 h in a vacuum oven at  $\sim 70$  °C. MIP analyses were performed, using a Thermo Finnigan Pascal Hg porosimeter (140 and 440 series), operating at a maximum pressure of 400 Mpa, capable of investigating macro-meso pores with radius between 58 and 0.0019 nm according to IUPAC [33 and references therein]. Data were processed by SOL.I.D (Solver of Intrusion Data), software (Ver. 1.6.6. – Thermo Scientific), allowing to determine real and bulk densities, Hg open porosity, total pore surface area, and average, median, and modal pore radius. The software creates automatically, for each instrument, a folder for Blank, for analyses (Data), for combined 140 and 240 or 440 files (Combi) and for analytical methods. The data files in SOL.I.D contain the raw data already corrected: 1) volume ( $\text{mm}^3/\text{g}$ ), already corrected by the blank subtraction and divided by the sample mass, 2) pressure (Mpa), already corrected by the hydrostatic pressure of mercury over the

sample.

The real density of binder (B) was indirectly determined, according to method suggested in literature [33], using the following general formula:

$$X_n(B) = [X_n(M) - (X_n(a) \times \% (a)) - (X_n(b) \times \% (b)) - (X_n(c) \times \% (c)) - (X_n(d) \times \% (d)) - (X_n(e) \times \% (e)) - (X_n(f) \times \% (f)) - (X_n(\cdot) \times \% (\cdot))] / \% (A)$$

where  $X_n(B)$  is the unknown property of binder to be determined (in this case the real density),  $X_n(M)$  is the real density of mortar sample and  $X_n(a) \times \% (a)$ ,  $(b)$  are the density and the percentage known from modal microscopic analysis and from literature (or determined experimentally) respectively.

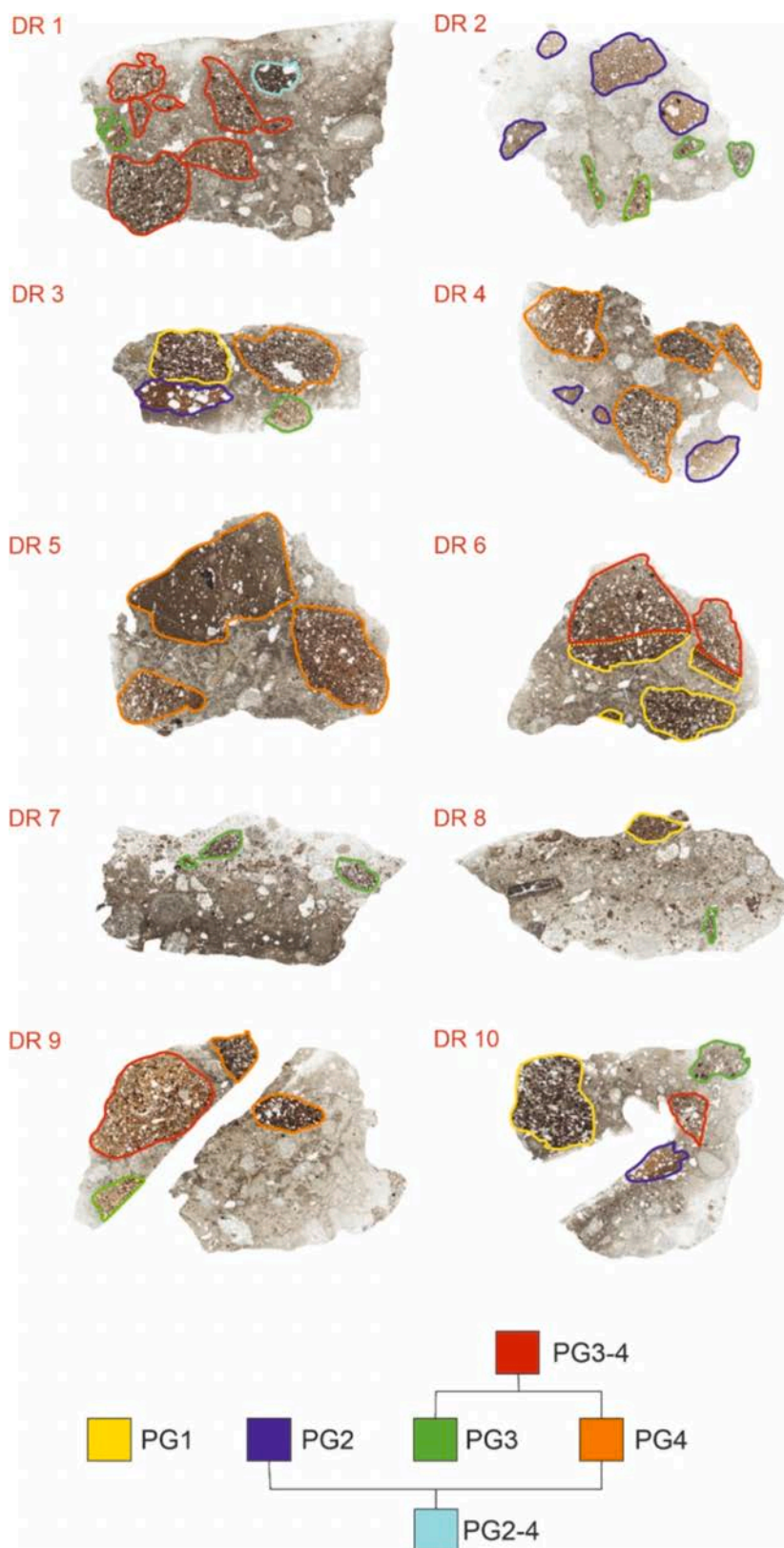
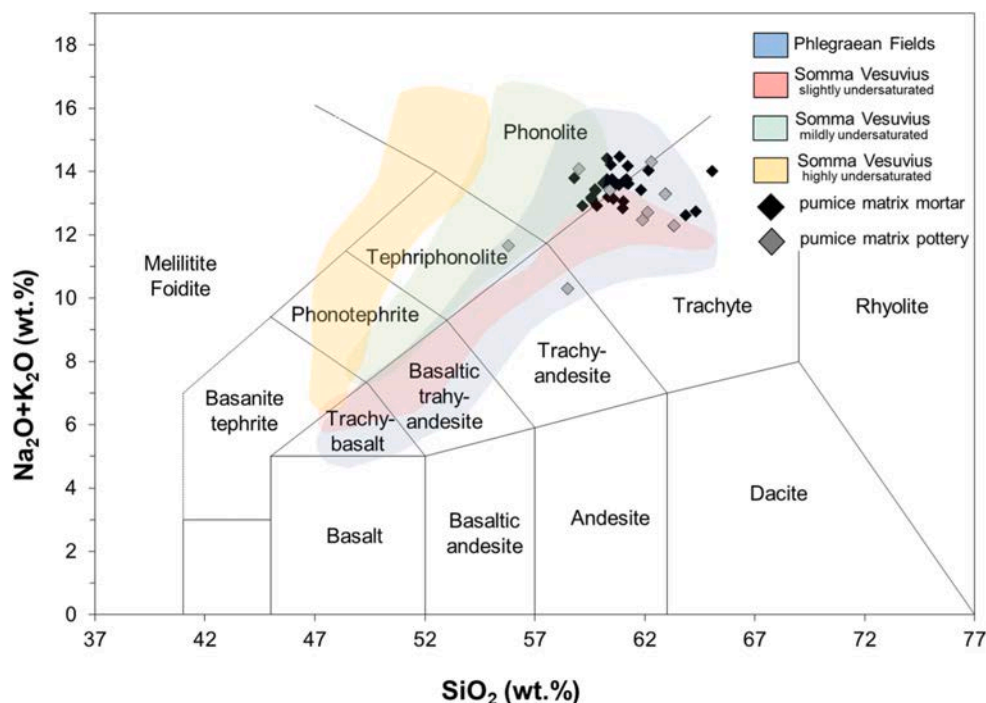


Fig. 3. Scanned thin section images of the investigated samples. Coloured contours of ceramics refer to the petrographic groups as indicated by the dendrogram.



**Table 2**  
Petrographic features of ceramic fragments.

Petrographic group	PG1	PG2	PG3	PG4
Samples	DR3, DR6, DR8, DR10	DR2, DR3, DR4, DR10	DR1, DR2, DR3, DR7, DR8, DR9, DR10	DR3, DR4, DR5, DR9
Optical activity of the ceramic matrix	active to inactive	active to weakly active	strongly active	active
Porosity	10–15%	5–10%	5–10%	5–10%
Shape	sub-rounded to weakly oriented	sub-rounded to elongated	sub-rounded to elongated	sub-rounded to elongated
Packing	25–30%	20–25%	Ca. 25%	20–25%
Grain size distribution	bimodal	bimodal	bimodal	bimodal
Inclusions	clinopyroxene, alkali feldspar, plagioclase, volcanic lithics (trachytes), pumice, glass shards, mica, garnet and leucite-bearing scoriae	alkali feldspar, plagioclase, volcanic lithics (trachytes), glass shards, grog, opaque minerals, mica	alkali feldspar, amphibole, clinopyroxene, volcanic lithics (trachytes), leucite-bearing scoriae, mica	alkali feldspar, clinopyroxene, plagioclase, volcanic lithics (trachytes), mica, pumice, grog, leucite



**Fig. 4.** TAS (Total Alkali vs. Silica; [42]) classification diagram for the analysed glassy pumice aggregates Phlegraean Fields and Somma Vesuvius data are from [27].

## 4. Results and discussion

### 4.1. Texture and petrography of mortars

Preliminary macroscopic observation of mortars showed that they occur in various hardness degrees, varying from intact, to quite dusty and to friable (Table 1). From a textural point of view, samples show an overall aggregate size ranging from fine- to coarse-grained.

According to optical microscopy observations, coating mortars showed a binder with a prevailing cryptocrystalline texture and a subordinately micritic (Fig. 2a).

Binder fraction also contains abundant subrounded lime lumps from millimetric to centimetric size (Fig. 2b). Lime lumps generally represent a non-reacted lime and their formation reasonably occurs during slaking process of lime, likely due to an insufficient setting of  $\text{Ca}(\text{OH})_2$  and/or a low water/lime ratio (usually 3,5/4:1); [36–38].

The mortars recipe in terms of aggregate, is the so-called *cocciopesto*, a typical building material frequently used in the ancient Rome for waterproof structures, such as cisterns and thermal baths [3]. The aggregate abundance ranges from 40% to 60%, as evaluated from comparative charts [39], and is mainly represented by ceramic fragments (Fig. 2c), volcanic fragments, pumice, and scoriae (Fig. 2d). Ceramic fragments appear different in terms of optical activity of the ceramic matrix, texture, and mineralogical composition (Fig. 2c). Secondary calcite on pore rims and pumice vesicles also occurs.

Volcanic aggregates consist of trachyte clasts (polycrystalline aggregates of dominant sanidine) and tuff fragments (various microcrystals dispersed in an ashy matrix). In addition, loose crystal fragments of sanidine, plagioclase, clinopyroxene and mica were also detected in the binder matrix.

Bedding mortars are characterized by binders with a prevailing micritic and subordinately cryptocrystalline texture (Fig. 2e). The

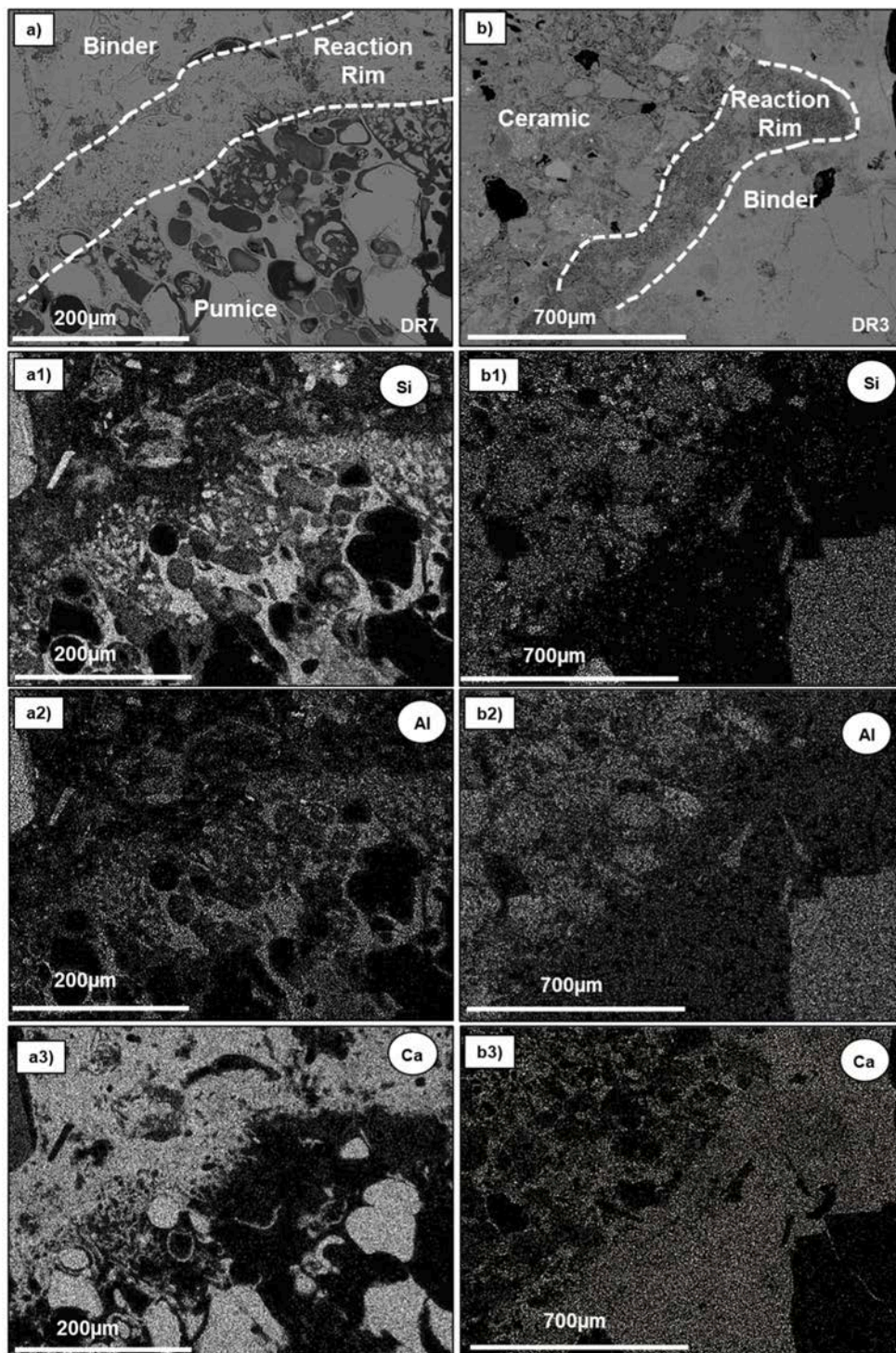


Fig. 5. BSE micrographs of a) DR7 and b) DR3 samples showing reaction rim between binder and pumice aggregates and elemental maps of Si, Ca and Al.

amount of millimetric lime lumps detected in this type of mortars is lower than that in coating mortars, testifying a greater degree of care/success in slaking of lime and in the mixing of raw materials. The aggregate fraction ranges from 30% to 40% and mainly consists of volcanic components (pumice, scoriae and volcanic lithics; Fig. 2f), along with rare ceramic fragments. Pumice shows evident reaction rims (Fig. 2f) and volcanic lithics are represented by trachyte and tuff. Sanidine, plagioclase, mica, and clinopyroxene were also identified in

the binder matrix.

#### 4.2. Petrographic description of ceramic fragments

Considering the heterogeneity of ceramic aggregates (coating mortars in particular), it was essential to carry out a detailed characterization of these aggregates.

The investigated ceramic fragments can be divided into four groups



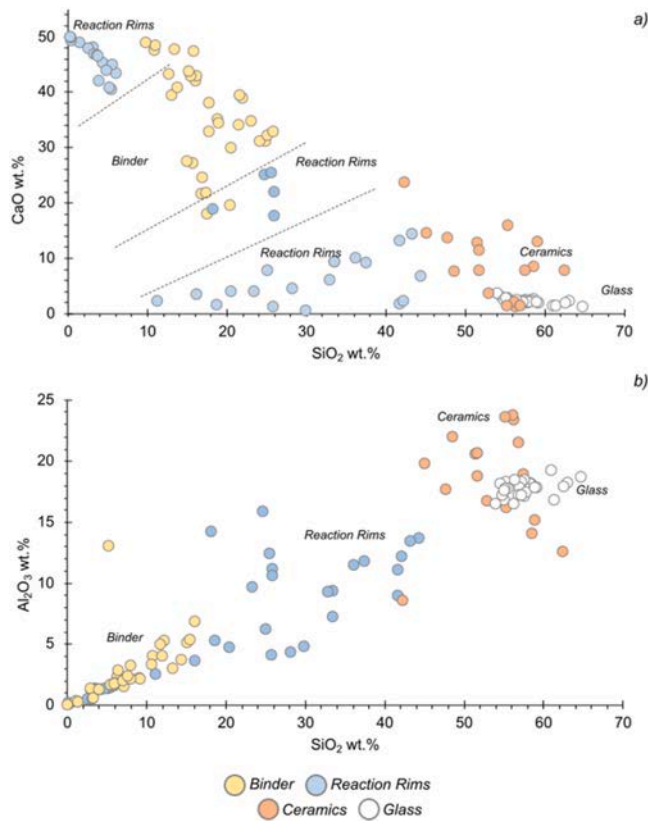


Fig. 6. a) CaO and b)  $\text{Al}_2\text{O}_3$  vs.  $\text{SiO}_2$  binary diagrams showing chemical differences between reaction elements. Glasses and matrix of ceramics (Supplementary Material S4 and S8) have been plotted for comparison.

Table 3  
Thermal analysis features of investigated samples.

Sample	SBW % 200–600 °C	$\text{CO}_2$ % 600–800 °C	$\text{CO}_2/\text{SBW}$	LOI
DR1	2.42	24.66	10.19	30.20
DR2	2.57	24.77	9.64	29.22
DR3	2.8	25.72	9.19	30.88
DR4	3.6	23.69	6.58	29.48
DR5	3.85	24.91	6.47	31.14
DR6	3.31	23.55	7.11	29.64
DR7	3.05	16.74	5.49	23.74
DR8	2.95	13.49	4.57	20.39
DR9	3.85	24.39	6.34	30.68
DR10	3.54	24.4	6.89	30.09

Abbreviations: LOI= Loss on Ignition; SBW= Structurally Bound Water.

(Fig. 3), based on their petrographic features, named Petrographic Group 1 (PG1) to 4 (PG4). Representative thin section images are shown in Supplementary Material (S1) for each Petrographic Group identified (Table 2). The features detected for each PG are reported in a synoptic table (Table 2) to highlight the differences between themselves. In detail, all PG show a bimodal distribution of grains and inclusions ranging from 20% to 30%. The optical activity of the ceramics body is extremely variable from strongly active to inactive, often even in the same PG. The main inclusions in ceramic fragments are characterized by alkali feldspar, plagioclase, mica, volcanic lithics (trachyte) and juvenile fragments (glass shards and pumice), whereas clinopyroxene (except for PG2) and amphibole identified only in PG3. In addition, the presence of some minerals, represented by leucite (PG1, PG3, PG4) and garnet (PG1) detected in some petrographic groups, may provide useful information on the origin of the raw material used to make the different ceramic

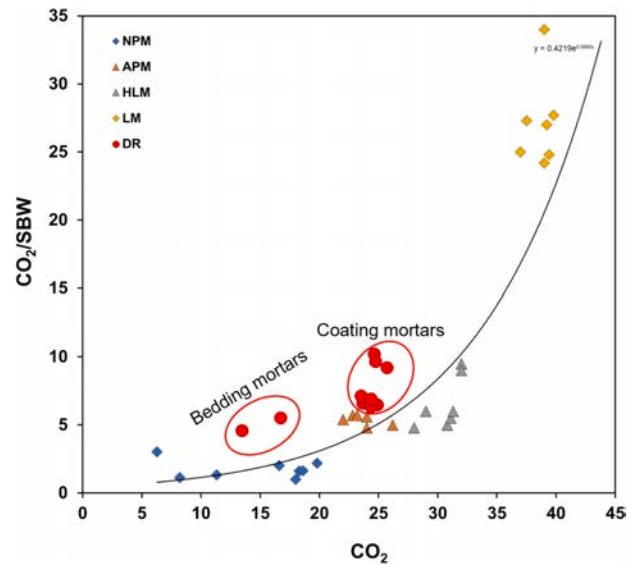


Fig. 7. Binary  $\text{CO}_2/\text{SBW}$  vs.  $\text{CO}_2$  (%) diagram comparing the obtained data from Dragonara cave (DR) and those of [37]. Abbreviations: NPM: natural pozzolanic mortars; APM: artificial pozzolanic mortars; HLM: hydraulic lime mortars; LM: lime mortars.

fragments.

Secondary calcite has been also observed in PG1, PG2 and PG3 mainly along the porosity and it increases at the ceramic aggregate-mortar boundary.

Moreover, other two intermediate Petrographic Groups have been identified, i.e., PG2–4 and PG3–4, showing combined mineralogical vs. petrographic features between groups 2–4 and groups 3–4, respectively.

### 4.3. Mineralogical, micro-structural and chemical characterization

#### 4.3.1. Binder and aggregates

Samples were separated in (1) binder and (2) aggregates (excluding ceramic fragments, due to their extreme variability), according to the UNI-EN 11305 [34]. XRPD results confirmed the occurrence of lime-based mortar with volcanic aggregate, as shown by semi-quantitative analyses reported in Supplementary Material 2 (S2).

Regarding binder phases, calcite is the most abundant phase with subordinate gypsum. The latter phase was detected in DR5 and DR8 and could be ascribed to sulphation processes of calcite due to pH decrease value, caused by dissolution of atmospheric  $\text{SO}_2$  [40].

According to XRPD analyses, aggregates contain fragments of Phlegraean tuff, with the typical zeolitic association phillipsite-chabazite-analcime [2,41] (de Gennaro et al., 1999; Colella et al., 2017), along with sanidine, pyroxene, and mica as pyrogenic phases. Quartz in all coating mortars is referred to inclusions in ceramic fragments.

EDS analyses showed a binder (Supplementary Material S3) is mainly composed of  $\text{CaO} + \text{MgO}$  varying from 24.4 to 50.3 wt%, with  $\text{SiO}_2 + \text{Al}_2\text{O}_3 + \text{FeO}$  sum varying from 0.4 to 23.0 wt%; lime lumps (Supplementary Material S4) are composed of prevailing  $\text{CaO}$ , with very high values of  $\text{CaO} + \text{MgO}$  (in the range 44.9–52.2 wt%) and lower  $\text{SiO}_2 + \text{Al}_2\text{O}_3 + \text{FeO}$  concentrations (in the range 0.18–5.99 wt%).

Regarding the provenance of volcanic aggregates raw materials, plotting their compositions (Supplementary Material S5) in the Total Alkali vs. Silica diagram (TAS; Fig. 4) for effusive volcanic rocks [42], the investigated pumice corresponds to trachyte-phonolite and do not show significant compositional differences (Fig. 4). Moreover, these chemical compositions are well consistent with that reported for the Phlegraean tuff [27].

Petrographic observations of ceramic fragments lead to hypothesize

**Table 4**Physical properties of coating mortars of wall layer and bedding mortar taken from *Dragonara* archaeological site performed by MIP.

Sample	Mortar function	$\rho_R$	$\rho_B$	$\Phi_O$ Hg	$pV$ Hg	$pA_{TOT}$	$pR_{AV}$	$pR_{MED}$	$pR_{MOD}$
		g/cm <sup>3</sup>	g/cm <sup>3</sup>	%	mm <sup>3</sup> /g	m <sup>2</sup> /g	μm	μm	μm
DR1	Coating	2.4710	1.6166	34.58	213.9	30.786	0.0139	0.0676	0.0996
DR9	Coating	2.5035	1.7321	30.81	177.9	15.633	0.0228	0.1018	0.1268
DR7	Bedding	2.2806	1.3675	40.04	292.77	60.48	0.0097	0.0194	0.0021

Abbreviation legend:  $\rho_R$  = real density;  $\rho_B$  = bulk density;  $\Phi_O$  Hg = mercury open porosity;  $pA_T$  = total pore surface area;  $pR_A$  = average pore radius;  $pR_{Me}$  = median pore radius,  $pR_{Mo}$  = modal pore radius.

**Table 5**

Compositional percentage distribution of binder and aggregates of coating and bedding mortar samples by modal analysis.

Sample	Mortar function	Binder		Aggregate									
		Lime matrix	Lime lumps	Ceramic fragment	Pumice Scoria	Trachytic clast	Tuff clast	Pl	Sd	Cpx	Mca	Qtz	Sum
		%	%	%	%	%	%	%	%	%	%	%	%
DR1	Coating	62	5	14	5	3	2.5	2.5	2	2	1.5	0.5	100
DR9	Coating	58	6	17	5	3	2.5	2.5	2	2	1.5	0.5	100
DR7	Bedding	71	3	11	4	2.5	2	2	1.5	1.5	1.5	-	100

Abbreviation legend: Pl = plagioclase; Sa = sanidine; Cpx = clinopyroxene; Mca = mica; Qz = quartz. Mineral abbreviations from [45].

**Table 6**Density values of binder and aggregate components of three coating and bedding mortar samples derived by literature and calculated absolute density and closed porosity ( $\Phi_C B$ ) of lime binder.

Sample	Mortar function	Binder			Aggregate								
		Lime matrix	$\Phi_C B$	Lime Lumps	Ceramic fragment	Pumice Scoria	Trachytic clast	Tuff clast	Pl	Sa	Cpx	Mca	Qtz
		g/cm <sup>3</sup>	%	g/cm <sup>3</sup>	g/cm <sup>3</sup>	g/cm <sup>3</sup>	g/cm <sup>3</sup>	g/cm <sup>3</sup>	g/cm <sup>3</sup>	g/cm <sup>3</sup>	g/cm <sup>3</sup>	g/cm <sup>3</sup>	g/cm <sup>3</sup>
DR1	Coating	2.44	10.0	2.71	2.69	2.52	2.56	2.54	2.65	2.53	3.40	3.10	2.65
DR9	Coating	2.48	8.6										
DR7	Bedding	2.19	19.3										

Pl = plagioclase; Sa = sanidine; Cpx = clinopyroxene; Mca = biotite; Qz = quartz. Mineral abbreviations from [45].

affinity among PG-1–3–4 and Somma-Vesuvius products. In fact, leucite-bearing scoriae and leucite crystals occur in almost all the petrographic groups of ceramics. Furthermore, the composition of the detected calcic garnet (solid solution between andradite 46–63% and grossular 22–29%) fits the composition of these minerals from the Somma-Vesuvius products, as reported in the literature [27]. Only the PG2 shows some differences in comparison with other PGs: in fact, (i) it is characterized by a bimodal distribution of grains and by the presence of sharp edged inclusions; (ii) it shows the lacking of garnet and/or leucite and/or leucite-bearing scoriae even if the composition of glasses detected in the ceramic matrix (Fig. 6) reflect the composition of the Campania volcanic district products [27].

#### 4.3.2. Reaction rims

Reaction rims (Fig. 5) have been generally observed at the interface between aggregate and binder fraction. Their presence has been detected through optical microscopy (cfr. 4.1) and was also confirmed using EDS chemical analyses (Supplementary Material S6).

These rims contain different amounts of CaO, as shown by Fig. 6a, depending essentially on availability, and thus activity, of silica of aggregates from which the rims form. On this base, three groups can be clearly distinguished for reaction rims, i.e. (i) CaO up to 14.3 wt%, (ii) 17.5 >CaO> 25.3 wt%, and (iii) CaO up to 49 wt%.

Chemical analyses of reaction rims show a progression, evidencing pozzolanic reaction. In this reaction, Si and Al come from both ceramic aggregates and pumice glass, while Ca is mainly provided by binder fraction.

Si and Al can react with Ca(OH)<sub>2</sub>, provided by binder, forming several gel phases, which differ from each other, based on the different

abundances of twocations and H<sub>2</sub>O. In this way, Calcium Silicate Hydrate (C-S-H) and/or Calcium Aluminate Silicate Hydrate (C-A-S-H) can form [43] depending on the aggregates composition (pumice glass and ceramics) and driving, the pozzolanic reaction. First reaction steps can be identified with early formation of reaction rims (Fig. 5a and b), when the alkaline solution begins to mobilize and leaching Si and Al provided by aggregates.

Based on the distribution of Si and Al inside the aggregates (i.e., belonging to mineralogical structures or making up the glass fraction), these elements can be leached in different amounts and, as reaction proceeds, an inverse correlation between SiO<sub>2</sub> and CaO amounts can be pointed out.

In this first step, Calcium Silicate Hydrate (C-S-H) can form if there is sufficient time of reaction.

As the reaction proceeds, also Al contributes to the formation of C-S-A-H gel which corresponds to rims with intermediate CaO content (i.e., 17.5 >CaO>25.3 wt%) and possibly represents the interfacial transition zone (ITZ, Supplementary Material S7) already described by literature [44]. Once the amount of Si is depleting (i.e., Si which can enter the reaction / take part to reaction), reaction rims exhibit an indirect enrichment of CaO (i.e., CaO content up to 49 wt% - Fig. 5).

Binary variation diagrams of Fig. 6a-b support the evidence discussed so far. Actually, as the reaction proceeds, and starting from the composition of glass and ceramics, SiO<sub>2</sub> decreases while CaO increases.

Moreover, the above described rims representing interfacial transition zone (ITZ) display also an Al<sub>2</sub>O<sub>3</sub> enrichment (6b, i.e. Ca(OH)<sub>2</sub> + Si → C-S-H and Ca(OH)<sub>2</sub> + Al → C-A-H).

Glass data were reported in Fig. 6 as reference for comparison.

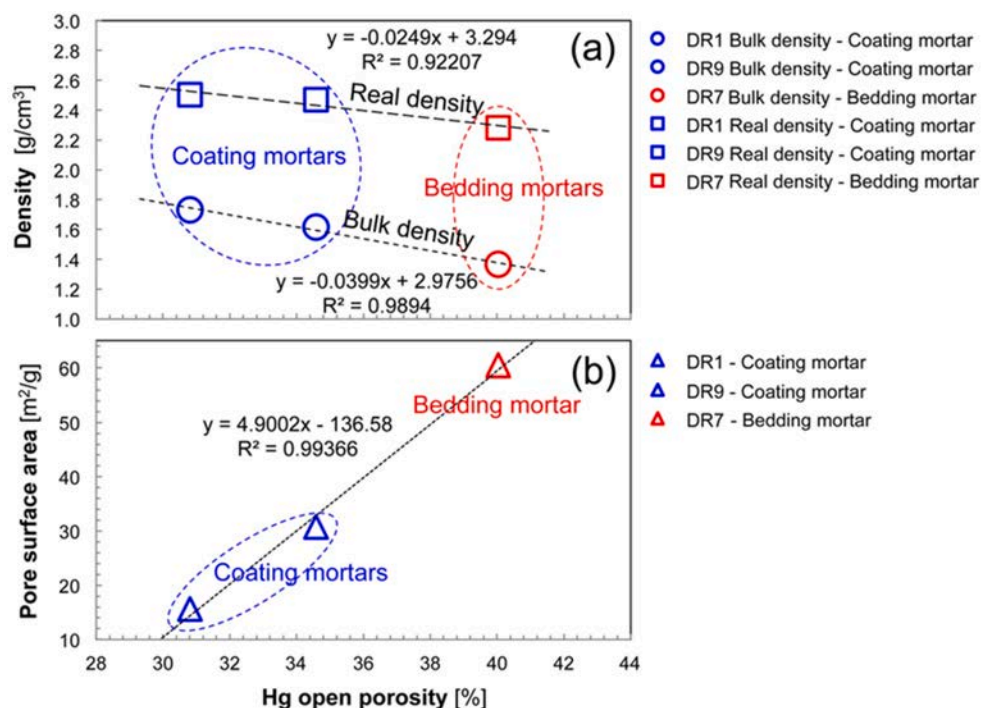


Fig. 8. Binary charts where plotted the main physical properties of mortar samples taken from *Dragonara* archaeological site. a) mercury open porosity ( $\Phi_{\text{O Hg}}$ ) vs. bulk density ( $\rho_{\text{B}}$ ) and open porosity ( $\Phi_{\text{O Hg}}$ ) vs. real density ( $\rho_{\text{R}}$ ); b) mercury open porosity ( $\Phi_{\text{O Hg}}$ ) vs. total pore surface area ( $\rho_{\text{A}_{\text{TOT}}}$ ).

#### 4.4. Hydraulic behaviour and pore system characterization

Chemical analyses highlighted the occurrence in the binder of newly formed hydraulic phases (C-A-S-H), while XRPD analyses confirmed the presence of gypsum.

The Hydraulicity Index (HI) calculated according to Boynton's formula  $(\text{SiO}_2 + \text{Al}_2\text{O}_3 + \text{Fe}_2\text{O}_3)/(\text{CaO} + \text{MgO})$  reported in literature [32] (S3) allowed us to consider the investigated lime lumps (S4) with low values of HI (0.04% on average) as aerial lime (quicklime). Bedding mortars (S3), showing averaged HI values of 0.65%, should be considered as highly hydraulic, whereas coating mortars (S3) show HI of 0.29% and thus are considered moderately hydraulic.

Considering these results, it is possible to infer that the coating mortars became hydraulic by addition of aggregates (volcanic materials and ceramic fragments) with peculiar features. These aggregates produced a "pozzolanic reaction", due to their silica and alumina content, that reacted with calcium hydroxide leading to the formation of calcium aluminium silicate hydrates (C-A-S-H phases) [17], furtherly testified and confirmed by reaction rims around pumice and ceramic fragment.

Thermal methods combined with mineralogical composition of the samples allowed us to obtain further information about the hydraulic characteristics of mortar samples. Investigated mortars (fraction < 63  $\mu\text{m}$ ) show a progressive loss of mass in the range of 40–1000  $^{\circ}\text{C}$ . All investigated samples are characterised by contents of structurally bound water (SBW) and  $\text{CO}_2$  typical of hydraulic mortars. In particular,  $\text{CO}_2/\text{SBW}$  ratio (Table 3; Fig. 7) allows us to classify mortars from *Dragonara* cave as "hydraulic" and, more specifically, to distinguish 1) bedding mortars as natural pozzolanic mortars from 2) coating mortars as artificial pozzolanic mortars [37].

#### 4.5. Physical properties of mortars

The different compositional features of two sample groups (coating and bedding mortars) reflect different physical properties (Table 4). Real density values are: 2.47–2.50  $\text{g}/\text{cm}^3$  for coating mortars (samples DR1,

DR9) and 2.28  $\text{g}/\text{cm}^3$  in bedding mortar (sample DR7, Table 4). This difference is related to the fact that real density is a parameter closely linked to type and compositional incidence of the solid phases in the mortars, and to a possible closed porosity present within the phases themselves (interphase) or in the matrix of the binder (intra-phase).

Coating mortars have an aggregate abundance of about 33–36 vol%, mainly characterized by ceramic fragments and subordinately by variably sized volcanic aggregates (pumice, scoriae and volcanic lithics) and low incidence of crystal-clasts components (i.e., sanidine, plagioclase, clinopyroxene, mica and quartz). Instead, bedding mortars are characterized by an aggregate presence of 26 vol%, consisting of the same kind of aggregate, with pumice and scoriae slightly variable in size, but less abundant ceramic fragments, if compared with coating mortars. Different compositional distribution of crystalline and amorphous (glassy) phases, obtained by modal microscopic analysis of three representative thin sections, are reported in Table 5. Thanks to these values, it is possible to understand the differences in real density values of two kind of mortars, mainly due to a greater percentage of high-density aggregates (ceramics: 2.69, lime lumps 2.68  $\text{g}/\text{cm}^3$ ) in coating mortars (Table 6).

The real density of mortar samples was indirectly determined [33] and reported in Table 6. The binder matrix of coating mortars shows a higher real density (2.44–2.48  $\text{g}/\text{cm}^3$ , Table 6) with respect to bedding mortar (2.19  $\text{g}/\text{cm}^3$ ), due to a different incidence of closed porosity (or with very thin pore radius) not accessible to Hg in MIP. Assuming that the density of the binder solid matrix is essentially that of calcite (2.71  $\text{g}/\text{m}^3$ ), it is possible to determine the closed porosity of the binder, which is different in the two cases: from 8.6% to 10% in coating mortars, and 19.3% in bedding mortar (Table 6). This difference is due to greater hydraulic degree of bedding mortars (as shown by TGA results), which leads to increased pore closure of the binder matrix.

As can be observed from Fig. 8a, bulk density, influenced by the real density and the total (open and closed) porosity, is higher in coating (2.47–2.50  $\text{g}/\text{cm}^3$ ) than in bedding mortars (2.28  $\text{g}/\text{cm}^3$ ), due to the higher presence of the ceramic component in the aggregate of the



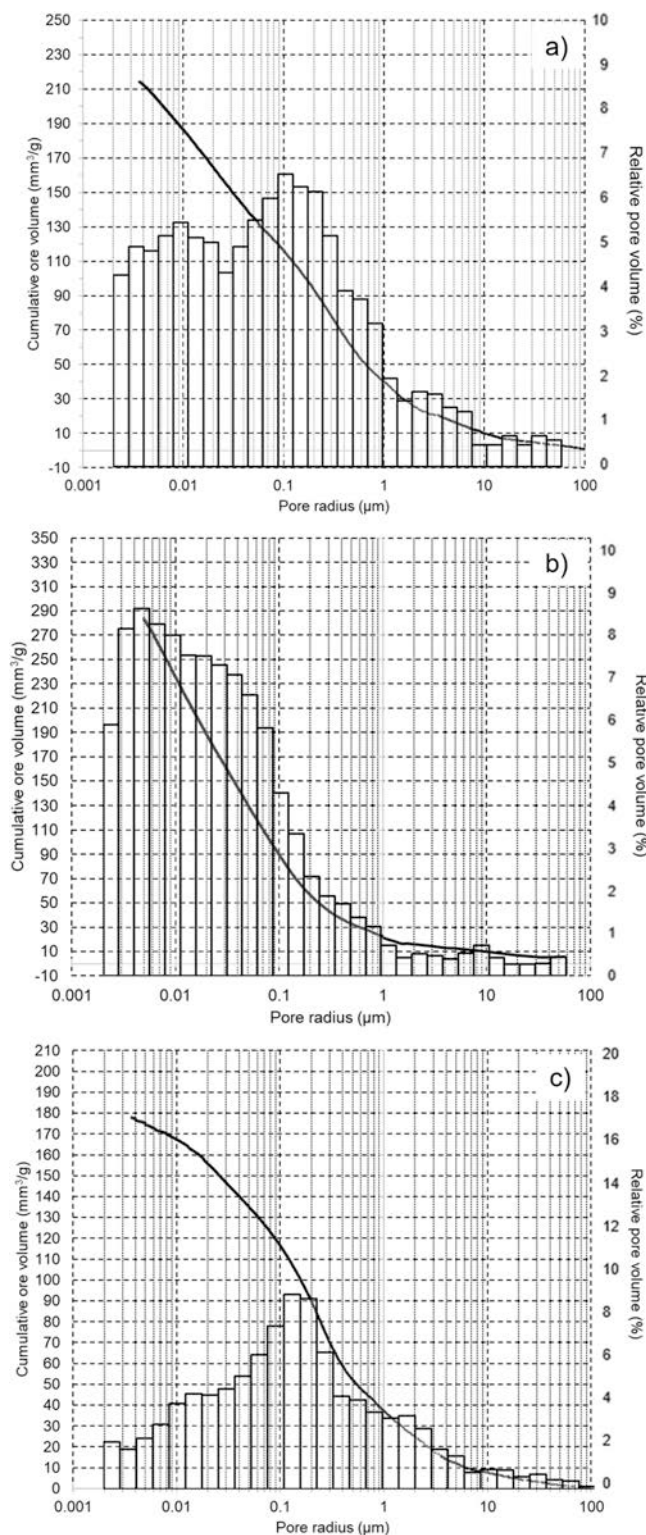


Fig. 9. Pore radius distribution (MIP) in *Dragonara* cave mortars. a - b) coating mortars DR1 and DR9; c) bedding mortar DR7.

former, and a lower amount of both open and closed porosity. Open porosity, ranging from 30.8 to 34.6 vol% in the coating mortars and 40% in the bedding mortar (Table 4), shows a clear negative correlation with both bulk density ( $R^2 = 0.99$ ) and real density ( $R^2 = 0.92$ ).

There is also a positive correlation ( $R^2 = 0.99$ ; Fig. 8b) between open porosity and total pore surface area ( $pA_{TOT}$ ), with values of the latter parameter of 15.6 and 30.7  $m^2/g$  in coating mortars and 60.5  $m^2/g$  in bedding mortars, respectively, due to the different compositional characteristics and laying of mortars related to their different technical function in the artefact.

For these latter reasons, two groups of mortars also show a different pore size features, characterised by a pore radius distribution centred in modal classes with  $pR_{MOD}$  of 0.10  $\mu m$  (sample DR9, Table 6, Fig. 9) and of 0.13  $\mu m$  (sample DR1, Table 6, Fig. 9) in the case of coating mortars, and much lower value in the bedding mortar (sample DR7, 0.0021  $\mu m$ , Table 4, Fig. 9), due to the greater incidence and hydraulic degree of the binder.

## 5. Conclusions

Mineralogical, petrographic, chemical, and microstructural investigations on mortar samples from the ancient *Dragonara* cave (Phlegraean Fields archaeological area, southern Italy) provided detailed information and compositional characteristics and thus on their mix-design. This research can be considered as a first methodological attempt to clarify the respective role of different aggregates used in ancient Roman mortars production and supplying further insights on production technology and features of the used raw materials.

- The compositional characteristics of the aggregates, both volcanic (pumice and scoriae) and of the crystalline fraction, dispersed in the mortar matrix (but also in the ceramic component), clearly indicate a local origin of the raw materials, being consistent with volcanic products from the Campania region (see 4.3.1).
- Considering the geological availability of volcanic material in the surrounding area of *Dragonara* cave, the high hydraulicity exhibited by all the studied mortars is due to 1) the values of the Hydraulicity Index (HI) and 2) the different reaction between the mortar and aggregates, both volcanic and ceramic. These values are the result of careful selection, preparation and mixing of the geomaterials used.
- The high hydraulicity is mainly due to the presence of volcanic material (mainly glass). The reaction edges are in fact predominantly present at the matrix-pumice interface rather than at the matrix-ceramic interface. Distribution of Si, Ca and Al varies systematically, starting from the unaltered (and unreacted) glass to the mortar matrix, forming distinct reaction zones with increasing Ca content: reaction rims (RR) to Interfacial Transition Zones (ITZ) and finally Ca-rich zones. The latter represent clear evidence of late-stage reactions.
- Bedding mortars exhibit 1) higher open porosity (40%) than coating mortars (33% on average), due to a higher presence of pumice and volcanic scoriae than ceramic fragments, and 2) higher closed porosity of the binder generated by the higher pozzolanic reactivity of the components (at the expense of the ceramic component). High amounts of low-density porous volcanic aggregates in bedding mortars also lead to lower values of real density ( $\sim 2.3 g/cm^3$ ) than in coating mortars ( $\sim 2.5$ ) and bulk density (2.28 vs. 2.47–2.50  $g/cm^3$ , respectively).

All the above considerations, obtained through the multi-analytical approach used in this work, allow us to hypothesize that, in the Phlegraean Fields archaeological site where it is located the *Dragonara* cave, the use of ceramic fragments was probably due to structural purposes, influencing the weight of the mortars, more than giving hydraulicity to the mortar mix design.

Finally, this work is part of a wider study and represents a starting point to plan future projects to compare our results with a larger dataset from the same archaeological and geological context. This aspect is fundamental to highlight the importance of the Roman mortars production technologies.

## Funding

This research did not receive any specific grant from funding agencies in the public, commercial, or not-for-profit sectors.

## CRedit authorship contribution statement

**Rispoli Concetta:** Writing – review & editing, Writing – original draft, Validation, Supervision, Methodology, Investigation, Formal analysis, Data curation, Conceptualization. **Montesano Giovanna:** Writing – review & editing, Writing – original draft, Visualization, Methodology, Investigation, Formal analysis, Data curation, Conceptualization. **Verde Maria:** Writing – review & editing, Writing – original draft, Methodology, Investigation, Formal analysis, Data curation, Conceptualization. **Balassone Giuseppina:** Visualization, Validation. **Columbu Stefano:** Writing – original draft, Methodology, Data curation. **De Bonis Alberto:** Writing – review & editing, Writing – original draft. **Di Benedetto Claudia:** Formal analysis, Data curation. **D’Uva Francesco:** Writing – original draft, Investigation, Data curation. **Esposito Renata:** Investigation, Conceptualization. **Graziano Sossio Fabio:** Writing – review & editing, Formal analysis, Data curation. **Mercurio Mariano:** Writing – review & editing, Resources, Methodology. **Morra Vincenzo:** Writing – review & editing, Validation, Resources. **Cappelletti Piergiulio:** Writing – review & editing, Visualization, Validation, Supervision, Resources, Investigation.

## Declaration of Competing Interest

The authors declare that they have no known competing financial interests or personal relationships that could have appeared to influence the work reported in this paper.

## Data availability

Data will be made available on request.

## Acknowledgements

The authors would like to thank the *Parco Archeologico dei Campi Flegrei* for the necessary authorisation and supervision during the sampling phase. We also thank Roberto de Gennaro for the invaluable assistance during EDS microanalyses and Sergio Bravi for his technical ability in thin section preparations. The authors would like to thank the journal editors and the anonymous reviewers for their useful comments that helped us in the revision of this manuscript.

## Data availability

All data generated or analysed during this study are included in this published article (and its [supplementary information files](#)).

## Appendix A. Supporting information

Supplementary data associated with this article can be found in the online version at [doi:10.1016/j.conbuildmat.2023.134408](https://doi.org/10.1016/j.conbuildmat.2023.134408).

## References

- M.R. Veiga, A.S. Silva, Mortars, in: B. Ghiassi, P.B. Lourenço (Eds.), Long-term Performance and Durability of Masonry Structures, Woodhead Publishing, 2019, pp. 169–208, <https://doi.org/10.1016/C2016-0-03710-5>.
- A. Colella, C. Di Benedetto, D. Calcaterra, P. Cappelletti, M. D’Amore, D. Di Martire, S.F. Graziano, L. Papa, M. de Gennaro, A. Langella, The Neapolitan Yellow Tuff: An Outstanding Example of Heterogeneity, *Constr. Build. Mater.* 136 (2017) 361–373, <https://doi.org/10.1016/j.conbuildmat.2017.01.053>.
- M. Collepardi, S. Collepardi, R. Troli. *Il nuovo calcestruzzo, sixth ed.*, Enco srl, 2016.
- D. Miriello, F. Antonelli, C. Apollaro, A. Bloise, N. Bruno, M. Catalano, S. Columbu, G.M. Crisci, R. De Luca, M. Lezzerini, S. Mancuso, A. La, Marca, A petro-chemical study of ancient mortars from the archaeological site of Kyme (Turkey), *Period. Miner.* 84 (2015) 497–517, <https://doi.org/10.2451/2015PM0028>.
- M. Lezzerini, S. Raneri, S. Pagnotta, S. Columbu, S. Gallelo, Archaeometric study of mortars from the Pisa’s Cathedral Square (Italy), *Measurement* 126 (2018) 322–331, <https://doi.org/10.1016/j.measurement.2018.05.057>.
- S. Raneri, S. Pagnotta, M. Lezzerini, S. Legnaioli, V. Palleschi, S. Columbu, N. F. Neri, P. Mazzoleni, Examining the reactivity of volcanic ash in ancient mortars by using a micro-chemical approach, *Mediterr. Archaeol. Archaeom. Int. Sci. J.* 18 (2018) 147–157, <https://doi.org/10.5281/zenodo.1285897>.
- G. Eramo, L. Spalluto, R. Laviano, Paving stones of the Via Traiana in Egnazia (Brindisi, 2nd A.D.): Provenance of stones [Il basolato della Via Traiana nel sito archeologico di Egnazia (Fasano, Br): provenienza dei materiali lapidei], *Rendiconti Online Società Geologica Italiana* 3, 2008, 357–358.
- M. Lezzerini, S. Legnaioli, G. Lorenzetti, V. Palleschi, M. Tamponi, Characterization of historical mortars from the bell tower of St. Nicholas church (Pisa, Italy), *Constr. Build. Mater.* 69 (2014) 203–212, <https://doi.org/10.1016/j.conbuildmat.2014.07.051>.
- D. Miriello, A. Bloise, G.M. Crisci, R. De Luca, B. De Nigris, A. Martellone, M. Osanna, R. Pace, A. Pecci, N. Ruggieri, New compositional data on ancient mortars and plasters from Pompeii (Campania – Southern Italy): Archaeometric results and considerations about their time evolution, *Mater. Charact.* 146 (2018) 189–203.
- M. Lezzerini, M. Spampinato, A. Sutter, N. Montevecchi, A. Aquino, Petrographic characteristics of the mortars from the Pisa’s Cathedral apse, *IMEKO TC4 International Conference on Metrology for Archaeology and Cultural Heritage, MetroArchaeo*, 2019, 459–463.
- F. Sitzia, M. Beltrame, S. Columbu, C. Lisci, C. Miguel, J. Mirão, Ancient restoration and production technologies of Roman mortars from monuments placed in hydrogeological risk areas: A case study, *Archaeol. Anthropol. Sci.* 12 (2020), 147, <https://doi.org/10.1007/s12520-020-01080-8>.
- G. Wei, C. Germinario, C. Grifa, X. Ma, Characterization of ancient building lime mortars of Anhui province, China: A multi-analytical approach, *Archaeometry* 62 (2020) 888–903, <https://doi.org/10.1111/arc.12565>.
- M.F. La Russa, S.A. Ruffolo, M. Ricca, N. Rovella, V. Comite, M.A. De Buergo, G. M. Crisci, D. Barca, Archaeometric approach for the study of mortars from the underwater archaeological site of Baia (Naples) Italy: preliminary results, *Period. Di Miner.* 84 (2015) 553–557, <https://doi.org/10.2451/2015PM0031>.
- C. Rispoli, A. De Bonis, V. Guarino, S.F. Graziano, C. Di Benedetto, R. Esposito, V. Morra, P. Cappelletti, The Ancient Pozzolan Mortars of the Thermal Complex of Baia (Campi Flegrei, Italy), *J. Cult. Herit.* 40 (2019) 143–154, <https://doi.org/10.1016/j.culher.2019.05.010>.
- C.M. Belfiore, R. Visalli, G. Ortolano, G. Barone, P. Mazzoleni, A GIS-based image processing approach to investigate the hydraulic behavior of mortars induced by volcanic aggregates, *Constr. Build. Mater.* 342 (Part B) (2022), <https://doi.org/10.1016/j.conbuildmat.2022.128063>.
- S. Dilaria, M. Secco, M. Rubinich, J. Bonetto, D. Miriello, D. Barca, G. Artioli, High-performing mortar-based materials from the late imperial baths of Aquileia: An outstanding example of Roman building tradition in Northern Italy, *Geoarchaeology* 37 (2022) 637–657, <https://doi.org/10.1002/gea.21908>.
- C. Rispoli, R. Esposito, L. Guerriero, P. Cappelletti, Ancient Roman Mortars from Villa del Capo di Sorrento: A Multi-Analytical Approach to Define Microstructural and Compositional Features, *Minerals* 11 (2021) 469, <https://doi.org/10.3390/min11050469>.
- C. Germinario, G. Cultrone, L. Cavassa, A. De Bonis, F. Izzo, A. Langella, M. Mercurio, V. Morra, P. Munzi, C. Grifa, Local production and imitations of Late Roman pottery from a well in the Roman necropolis of Cuma in Naples Italy, *Geoarchaeology* 34 (2019), <https://doi.org/10.1002/gea.21703>.
- C. Germinario, G. Cultrone, L. Cavassa, A. De Bonis, F. Izzo, A. Langella, M. Mercurio, V. Morra, P. Munzi, Grifa, Local production and imitations of Late Roman pottery from a well in the Roman necropolis of Cuma in Naples, Italy, *Geoarchaeology* 34 (2019) 62–79, <https://doi.org/10.1002/gea.21703>.
- C. Scarpati, P. Cole, A. Perrotta, The neapolitan yellow tuff-a large volume multiphase eruption from Campi Flegrei, Southern Italy, *Bull. Volcano* 55 (1993) 343–356, <https://doi.org/10.1007/BF00301145>.
- L. Pappalardo, L. Civetta, M. D’Antonio, A. Deino, M. Di Vito, G. Orsi, A. Carandente, S. de Vita, R. Isaia, M. Piochi, Chemical and Sr-isotopic evolution of the Phlegrean magmatic system before the Campanian Ignimbrite and the Neapolitan Yellow Tuff eruptions, *J. Volcanol. Geotherm. Res.* 91 (1999) 141–166, [https://doi.org/10.1016/S0377-0273\(99\)00033-5](https://doi.org/10.1016/S0377-0273(99)00033-5).
- C. Scarpati, A. Perrotta, S. Lepore, A. Calvert, Eruptive history of Neapolitan volcanoes: Constraints from  $^{40}\text{Ar}$ - $^{39}\text{Ar}$  dating, *Geol. Mag.* Vol.150 (3) (2013) 412–425, <https://doi.org/10.1017/S0016756812000854>.
- B. Giaccio, I. Hajdas, R. Isaia, A. Deino, S. Nomade, High-precision  $^{14}\text{C}$  dating and  $^{40}\text{Ar}$ - $^{39}\text{Ar}$  dating of the Campanian Ignimbrite (Y-5) reconciles the time-scales of climatic-cultural processes at 40 ka, *Sci. Rep.* 7 (2017), 45940, <https://doi.org/10.1038/srep45940>.
- A.L. Deino, G. Orsi, S. de Vita, P. Piochi, The age of the Neapolitan yellow tuff caldera-forming eruption (Campi Flegrei caldera-Italy) assessed by  $^{40}\text{Ar}$ - $^{39}\text{Ar}$  dating method, *J. Volcano Geotherm. Res.* 133 (2004) 157–170, [https://doi.org/10.1016/S0377-0273\(03\)00396-2](https://doi.org/10.1016/S0377-0273(03)00396-2).
- G. Orsi, S. de Vita, M. Di Vito, The restless, resurgent Campi Flegrei nested caldera (Italy): constraints on its evolution and configuration, *J. Volcanol. Geotherm. Res.* 74 (1996) 179–214, [https://doi.org/10.1016/S0377-0273\(96\)00063-7](https://doi.org/10.1016/S0377-0273(96)00063-7).

- [26] Servizio Geologico d'Italia, Geological map of Italy, F 465 Isola di Procida. 1:25000 – ISPRA Geological Survey of Italy, ISPRA Roma, 2012. <https://www.isprambiente.gov.it/en/projects/soil-and-territory/carg-project-geologic-and-geothematic-cartography>.
- [27] V. Morra, D. Calcaterra, P. Cappelletti, C. Colella, L. Fedele, R. de Gennaro, A. Langella, M. Mercurio, M. de Gennaro, Urban Geology: Relationships between Geological Setting and Architectural Heritage of the Neapolitan Area, *J. Virtual Explor.* 36 (2010).
- [28] M.A. Di Vito, R. Isaia, G. Orsi, J. Southon, S. de Vita, M. D'Antonio, L. Pappalardo, M. Piochi, Volcanism and deformation since 12000 years at the Campi Flegrei caldera (Italy), *J. Volcanol. Geotherm. Res.* 91 (1999) 221–246, [https://doi.org/10.1016/S0377-0273\(99\)00037-2](https://doi.org/10.1016/S0377-0273(99)00037-2).
- [29] P. Amalfitano, G. Comodeca, M. Medri, I. Campi Flegrei, un itinerario archeologico. Maersilio ed. Venezia, 1990.
- [30] R. Di Bonito R. Giammelli, *Le Terme Dei Campi Flegrei – Milano, Roma, 1992*.
- [31] L. Fedele, D.D. Insinga, A.T. Calvert, V. Morra, A. Perrotta, C. Scarpati,  $^{40}\text{Ar}/^{39}\text{Ar}$  dating of tuff vents in the Campi Flegrei calder (Southern Italy): toward a new chronostratigraphic reconstruction of the Holocene volcanic activity, *Bull. Volcano* 73 (2011) 1323–1336, <https://doi.org/10.1007/s00445-011-0478-8>.
- [32] R.S. Boynton. *Chemistry and Technology of Lime and Limestone*, 2nd ed., John Wiley & Sons., New York, NY, USA, 1980, p. 1980.
- [33] S. Columbu, A.M. Garau, Mineralogical, petrographic, and chemical analysis of geomaterials used in the mortars of Roman Nora theatre (south Sardinia, Italy), *Ital. J. Geosci.* 136 (2017) 238–262, <https://doi.org/10.3301/IJG.2017.05>.
- [34] UNI-EN 11305:2009 Beni culturali: Malte storiche, linee guida per la caratterizzazione mineralogico petrografica, fisica e chimica delle malte.
- [35] UNI EN 12407:2019 Natural stone test methods - Petrographic examination.
- [36] A. Bakolas, G. Biscontin, V. Contardi, E. Francesehi, A. Moropoulou, D. Palazzi, E. Zendri, Thermoanalytical research on traditional mortars from Venice, *Thermochim. Acta* 269/270 (1995) 817–828, [https://doi.org/10.1016/0040-6031\(95\)02574-X](https://doi.org/10.1016/0040-6031(95)02574-X).
- [37] A. Moropoulou, A. Bakolas, S. Anagnostopoulou, Composite materials in ancient structures, *Cem. Concr. Compos.* 27 (2005) 295–300, <https://doi.org/10.1016/j.cemconcomp.2004.02.018>.
- [38] L. Barba, J. Blancas, L.R. Manzanilla, A. Ortiz, D. Barca, G.M. Crisci, D. Miriello, A. Pecci, Provenance of the limestone used in Teotihuacan (Mexico): A methodological approach, *Archaeometry* 51 (2009) 525–545, <https://doi.org/10.1111/j.1475-4754.2008.00430.x>.
- [39] R.D. Terry, G.V. Chilingar, Summary of concerning some additional aids studying sedimentary formations, *J. Sediment. Petrol.* 25 (1955) 229–234, <https://doi.org/10.1306/74D70466-2B21-11D7-8648000102C1865D>.
- [40] M. de Gennaro, M.D. Fuscaldò, C. Colella, Weathering mechanisms of monumental tuff-stone masonry in downtown of Naples, *Sci. Tech. Cult. Herit.* 2 (1993) 53–62.
- [41] M. de Gennaro, A. Inconronato, G. Mastrolorenzo, M. Adabbo, G. Spina, Depositional mechanisms, and alteration processes in different types of pyroclastic deposits from Campi Flegrei Volcanic Field (Southern Italy), *J. Volcanol. Geotherm. Res.* 91 (1999) 303–320, [https://doi.org/10.1016/S0377-0273\(99\)00040-2](https://doi.org/10.1016/S0377-0273(99)00040-2).
- [42] M.J. Le Bas, R.W. Le Maitre, A. Streckeisen, B.A. Zanettin, Chemical Classification of Volcanic Rocks Based on the TotalAlkali-Silica Diagram, *J. Petrol.* 27 (1986) 745–750.
- [43] G. Artioli, M. Secco, A. Addis, The Vitruvian legacy: mortars and binders before and after the Roman world, *EMU Notes Mineral.* 20 (2019) 151–202.
- [44] V. Nezerka, J. Nemecek, Z. Slizkova, P. Tesarek, Investigation of crushed brick-matrix interface in lime-based ancient mortar by microscopy and nanoindentation, *Cem. Concr. Compos.* 55 (2014) 122–128, <https://doi.org/10.1016/j.cemconcomp.2014.07.023>.
- [45] D.L. Whitney, B.W. Evans, Abbreviations for names of rock-forming minerals, *Am. Mineral.* (2010) 185–187, <https://doi.org/10.2138/am.2010.3371>.